Mon. Not. R. Astron. Soc. **329,** 277–289 (2002)

Infrared magnitude–redshift relations for luminous radio galaxies

K. J. Inskip,[1★] P. N. Best,[2,3] M. S. Longair[1] and D. J. C. MacKay[1]

[1]*Cavendish Astrophysics Group, Cavendish Laboratory, Madingley Road, Cambridge CB3 0HE*
[2]*Sterrewacht Leiden, Postbus 9513, 2300 RA Leiden, the Netherlands*
[3]*Institute for Astronomy, Royal Observatory Edinburgh, Blackford Hill, Edinburgh EH9 3HJ*

Accepted 2001 September 4. Received 2001 August 30; in original form 2001 April 10

ABSTRACT

Infrared magnitude–redshift relations (K–z relations) for the 3CR and 6C samples of radio galaxies are presented for a wide range of plausible cosmological models, including those with non-zero cosmological constant Ω_Λ. Variations in the galaxy formation redshift, metallicity and star formation history are also considered. The results of the modelling are displayed in terms of magnitude differences between the models and no-evolution tracks, illustrating the amount of K-band evolution necessary to account for the observational data.

Given a number of plausible assumptions, the results of these analyses suggest that: (i) cosmologies which predict $T_0H_0 \gtrsim 1$ (where T_0 denotes the current age of the Universe) can be excluded; (ii) the star formation redshift should lie in the redshift interval $5 \leq z_f \leq 20$, values towards the lower end of the range being preferred in cosmologies with larger values of T_0H_0; (iii) the Einstein–de Sitter model ($\Omega_0 = 1, \Omega_\Lambda = 0$) provides a reasonable fit to the data; and (iv) models with finite values of Ω_Λ can provide good agreement with the observations only if appropriate adjustments of other parameters such as the galaxy metallicities and star formation histories are made. Without such modifications, even after accounting for stellar evolution, the high-redshift radio galaxies are more luminous (that is, more massive) than those nearby in models with finite Ω_Λ, including the favoured model with $\Omega_0 = 0.3, \Omega_\Lambda = 0.7$. For cosmological models with larger values of T_0H_0, the conclusions are the same regardless of whether any adjustments are made or not. The implications of these results for cosmology and models of galaxy formation are discussed.

Key words: galaxies: active – galaxies: evolution – cosmological parameters – radio continuum: galaxies.

1 INTRODUCTION

The models used to account for the infrared magnitude–redshift relation of luminous radio galaxies are sensitive to the assumptions made concerning the evolution of their stellar content, as well as to the choice of cosmological model. Galaxies at a particular redshift are observed at different cosmic epochs in different cosmological models and so their predicted spectra at a given redshift can vary quite dramatically. Accurate modelling of the evolution of galaxy spectra with cosmic time is required if the infrared K magnitude–redshift relation is to be used to constrain the range of acceptable world models. In this paper the spectral evolution of galaxies is modelled for different plausible cosmological models using the most recent spectral synthesis codes of Bruzual & Charlot (in preparation), GISSEL2000, and these results are compared with the observational data. Even for the simplest cases, numerous cosmological and evolutionary effects need to be taken into account, and it is often not intuitively obvious how changes in the assumptions made will change the predicted relations – one of the objectives of this paper is to provide insights to this. Although our prime concern is the K–z relation for radio galaxies, the considerations of this paper are relevant to all such cosmological studies.

The radio galaxies associated with the most powerful extragalactic radio sources seem to form a remarkably uniform class of galaxy out to large redshifts. Following the early work of Lilly & Longair (1984), Best, Longair & Röttgering (1998a) carried out a much more detailed analysis of the photometric properties of a complete sample of 3CR radio galaxies (the brightest radio galaxies in the northern sky selected at 178 MHz; Laing, Riley & Longair 1983). They modelled the K–z relation for world models with $\Omega_0 = 0$ and $\Omega_0 = 1$, in both cases assuming $\Omega_\Lambda = 0$. These models included passive evolution of the stellar populations of the galaxies with formation redshifts of 3, 5 and 20. The passive evolution models in the $\Omega_0 = 1$ universe provided a reasonable fit to the observations, whereas those with $\Omega_0 = 0$ gave a poor fit. The

★E-mail: kji@mrao.cam.ac.uk

models with low redshifts of formation, $z_f \approx 3$, resulted in galaxies more luminous than those observed at $z \gtrsim 1.2$, suggesting that the stellar populations of the galaxies must have formed at $z > 3$.

Eales & Rawlings (1996) and Eales et al. (1997) determined the K–z relation for a complete sample of 6C radio galaxies which were selected at 151 MHz and are about six times fainter in flux density than the 3CR sample (Eales 1985). The 6C host galaxies have similar K luminosities to those of the 3CR galaxies at $z \lesssim 0.8$, but are about 0.6 mag fainter at larger redshifts. Nevertheless, the high-redshift 6C galaxies are significantly brighter than expected in world models in which no evolution of the stellar populations of the galaxies is assumed.

The objectives of this paper are to review the current status of the K–z relation for 3CR and 6C luminous radio galaxies (Section 2) and then to carry out a more extensive analysis of the resulting K–z relation for a wider range of plausible world models than those considered by Best et al. (1998a) and Eales et al. (1997), including models with a non-zero cosmological constant. The predicted evolution of the stellar populations of the galaxies is derived from the most recent spectral synthesis codes of Bruzual & Charlot (1993, and in preparation), GISSEL2000; a wide range of stellar synthesis models is considered, as well as the effects of changes in metallicity. The details of the different cosmological models, the spectral synthesis codes and procedures used to predict the K–z relations are described in Section 3. The results of these calculations are described in Section 4, indicating which parameters have the greatest impact upon the form of the predicted K–z relation. Also included in that Section are the results of varying the star formation history and metallicity in plausible ways. Most massive galaxies at small redshifts have high metallicities and colour–magnitude relations show that more massive galaxies are redder in colour, suggesting a mass–metallicity correlation (see, for example, Arimoto & Kodama 1996). On the other hand, at high redshifts, we might expect a lower metal content, as suggested by the analyses of Pei, Fall & Hauser (1999) and Pettini et al. (1997). In Section 5 the results of these analyses are discussed, and our conclusions are summarized in Section 6. Throughout the paper, $H_0 = 50\,\mathrm{km\,s^{-1}\,Mpc^{-1}}$ is adopted, unless otherwise stated.

2 THE K–z RELATION FOR LUMINOUS RADIO GALAXIES

2.1 The revised K–z diagram

The observational data used in this analysis consist of infrared K magnitudes for 72 3CR galaxies in the redshift interval $0 < z < 1.8$ (Best et al. 1998a), and 57 6C galaxies in the range $0 < z < 3.4$ (Eales & Rawlings 1996; Eales et al. 1997). The 3CR galaxies comprise a complete sample of radio sources with flux densities $S_{178} \geq 10.9$ Jy at 178 MHz, with a mean flux density of about 15 Jy; the 6C sample is complete in the flux density interval $2.2 \leq S_{151} \leq 4.4$ Jy at 151 MHz, with an equivalent mean flux density at 178 MHz of about 2.6 Jy. The 3CR K magnitudes were obtained for $z < 0.6$ from observations with the IRCAM3 array on the UK Infrared Telescope (UKIRT; Best, Longair & Röttgering 1997), and for $z < 0.6$ from the photometry of Lilly & Longair (1984). The 6C data points were mostly derived from IRCAM observations, but also from colour corrected K' observations with the REDEYE camera of the Canada–France–Hawaii Telescope (Eales et al. 1997).

Various factors had to be included to create a self-consistent set of K magnitudes. First, aperture corrections were made, reducing the magnitudes to a standard circular aperture of metric diameter 63.9 kpc. These aperture corrections are dependent on the cosmological model, because of the differences in the angular diameter versus redshift relation; however, the changes from the standard $\Omega_0 = 1$, $\Omega_\Lambda = 0$ model are generally small, $\lesssim$0.1 mag, and so the data were converted to 63.9 kpc in the $\Omega_0 = 1$, $\Omega_\Lambda = 0$ model, and the model-to-model variations were included in the predicted model tracks.

The 63.9 kpc aperture was chosen because it had been adopted for the 6C observations wherever possible. In cases where there was a nearby companion galaxy, or if other problems prevented the use of the full aperture, magnitudes for the 6C galaxies were determined for smaller apertures and aperture corrections were applied by Eales et al. (1997); for galaxies at redshifts $z < 0.6$ they assumed that the radio galaxies follow an elliptical galaxy growth curve (Sandage 1972), and at redshifts $z > 0.6$ they assumed that the growth curve for the luminosity L of the galaxy within radius r could be represented by $L(< r) \propto r^{0.35}$. The K magnitudes of the 3CR galaxies were originally determined within a 9-arcsec diameter aperture. At large redshifts, this is almost equivalent to 63.9 kpc, and so the aperture corrections were small. Larger aperture corrections were necessary at low redshifts because the 9-arcsec aperture included only the central regions of the galaxy (Lilly & Longair 1984). A de Vaucouleurs profile for giant ellipticals was used to correct these magnitudes to the standard diameter, as the analysis of Best et al. (1998a) showed that this is a good representation of the variation of the K surface brightness with radius. It is also consistent with the radial optical light profile found for low-redshift radio galaxies by Lilly, McLean & Longair (1984).

The resulting K–z relation for 3CR and 6C galaxies, represented by open boxes and crosses respectively, is shown in Fig. 1. New versions of the predicted K–z relations are shown for an $\Omega_0 = 1$, $\Omega_\Lambda = 0$ world model. These involve the use of the most recent set of spectral synthesis codes (GISSEL2000), for which a Scalo Initial Mass Function was adopted, with upper and lower mass cut-offs of 100 and 0.1 $M_\odot$ respectively; solar metallicity was assumed. In addition, improved K-band transmission data for the K-band filter of UKIRT were used. Details of these procedures are discussed in Section 3.2. The differences as compared with the analysis carried out by Best et al. (1998a) are very small, and so their conclusions for the $\Omega_0 = 0$ and $\Omega_0 = 1$ models are unchanged. In particular, the $\Omega_0 = 1$, $\Omega_\Lambda = 0$ model with passive evolution of the stellar content of the galaxies provides a satisfactory fit to the observations and will be used as a fiducial model in the new computations.

2.2 The 3CR, 6C and MRC radio galaxies

One of the intriguing features of the comparison of the 3CR and 6C data is that, although they are in excellent agreement at redshifts $z < 0.6$, there is a progressive shift in their mean magnitudes at greater redshifts; the mean K magnitude of the 6C galaxies at $z > 1$ is about 0.6 mag fainter on average than the 3CR galaxies (Eales et al. 1997). This can be seen in Fig. 1, where the boxes, representing 3CR galaxies, lie towards the low limit of the distribution of the crosses, representing 6C galaxies, at $z > 1$.

Given the quite large dispersion about the mean K–z relation, Bayesian statistics have been used to investigate the significance of this magnitude difference and how it evolves with redshift without making restrictive assumptions about the underlying distribution

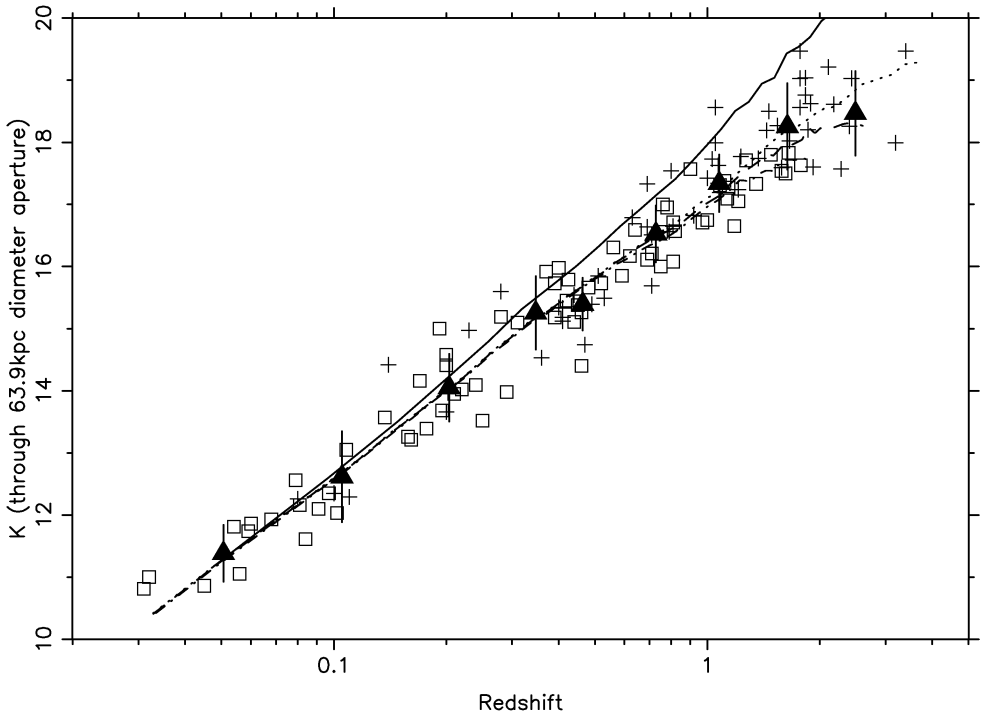

Figure 1. The revised K–z diagram for powerful radio galaxies for the world model with $\Omega_0 = 1$, $\Omega_\Lambda = 0$. The open squares represent 3CR galaxies and the crosses 6C galaxies. The solid curve corresponds to the predicted K–z relation for a non-evolving stellar population. The three other relations are for passively evolving galaxies in which the stellar population formed at a constant rate for an initial period of 1 Gyr. The three formation redshifts were: $z_f = 3$, dot-dashed line; $z_f = 5$, dashed line; and $z_f = 20$, dotted line. The solid triangles show mean values of the K magnitudes for both the 3CR and 6C data averaged in intervals of $0.1T_0$, where T_0 is the age of the world model, $T_0 = 2/3H_0$ for this case. The bars show the standard deviation of the distribution of magnitudes in each of these bins.

(see Fig. 2). The results clearly show the mean difference between the two data sets of about 0.6 mag at high redshift/early times and its decrease to zero at later times. The mean value of $\delta y(x)$ increases slightly at the lowest redshifts to about 0.15 mag, but this increase is not significant. At high redshifts the difference in K magnitudes between 3CR and 6C galaxies is significant at the 95 per cent confidence limit.

This result for the 6C galaxies is mirrored by that of the still fainter 7C radio galaxies (Willott, private communication). However, McCarthy (1999) and van Breugel et al. (1998) have studied the K–z relation for radio galaxies in the MRC 1-Jy sample, which contains sources with flux densities $S_{408} > 1$ Jy at 408 MHz ($\equiv S_{178} \sim 5.8$ Jy) from the Molonglo reference catalogue (McCarthy et al. 1996), and they find that the mean K-band magnitudes of the MRC radio galaxies to be only 0 to 0.2 mag fainter than the 3CR, a much smaller difference than for the 6C sources. The ~25 per cent spectroscopic incompleteness of this sample may introduce a bias, in that it is more difficult to obtain redshifts for intrinsically fainter galaxies, but McCarthy argues that this bias is unlikely to be sufficiently great to alter the mean magnitude of the MRC galaxies by 0.6 magnitudes.

The important aspect of this discussion is whether or not there is a correlation between radio luminosity and K-absolute magnitude, as would be the case if it is accepted that there is a real difference between the K–z diagrams for the 3CR and 6C samples. For the purpose of the present analysis, we have assumed that the difference between the 6C and 3CR samples, being smaller than the scatter within either sample, can be ignored. Therefore, we have taken mean values and dispersions for the combined sample. These are indicated by the solid triangles and associated error bars in Fig. 1.

A literal interpretation of the K–z diagram shown in Fig. 1 suggests that to a good approximation the luminous radio galaxies belong to a single population of passively evolving galaxies of the same stellar mass. The galaxies also have the same characteristic radii of about 10 kpc over the entire range $0 < z < 1.5$ (Best et al. 1998a, McLure & Dunlop 2000), which supports this conclusion. As discussed by Best et al., this is a somewhat surprising result, since the preferred hierarchical clustering picture of galaxy formation predicts that the masses and radii of galaxies would grow significantly over the redshift range considered. Evidence suggests that galaxy environments also differ with redshift; high-redshift 3CR galaxies seem to belong to protocluster environments, whereas low-redshift galaxies are more commonly found in small groups or otherwise isolated environments. Intuitively, it seems difficult to reconcile these points with closed-box passive evolution of the stellar populations of the 3CR galaxies. Best et al. recognized this problem and argued that the luminous radio galaxies must be observed at a similar stage in their evolution, specifically that at which they had attained a certain stellar mass. Provided that stars brought together by ongoing mergers were formed at the same early epoch, the old stellar populations of galaxies formed by hierarchical clustering would appear to be passively evolving. The small scatter in the colour–magnitude relations of elliptical galaxies observed out to redshifts $z \sim 1$ (Bower, Kodama & Terlevich 1998; Stanford, Eisenhardt & Dickinson 1998) justifies this assumption.

A further objective of our analysis is to determine whether it remains true that the luminous galaxies present on the K–z relation have the same stellar mass, and how different assumptions about the underlying cosmology and the evolution of the stellar populations change this conclusion.

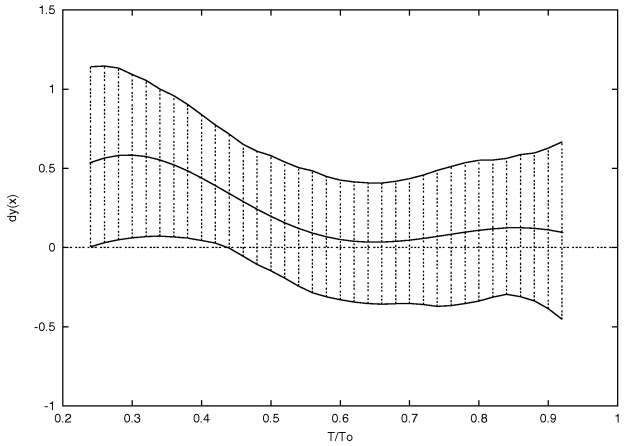

Figure 2. The inferred K-band magnitude difference [d$y(x)$] between the 3CR and 6C galaxy populations as a function of cosmic time, expressed as a fraction of T_0, the present age of the universe, determined using a Bayesian statistical approach. In the Bayesian approach two flexible distributions for the reduced magnitude $y(x)$ (the difference between the observed magnitudes K and the expectation K_0 of the no-evolution model) are assumed to underlie the two data sets for the range of redshifts covered by both samples. $y(x)$ is represented by a sum of Legendre polynomials Φ such that $y(x) = \Sigma_h w_h \Phi_h(x)$. Similarly, the scatter in the observational data $\sigma(x)$ is represented by $\log_{10}\sigma(x) = \Sigma b_h \Phi_h(x)$. The differences between the two data sets and their scatter are defined by the quantities $\delta y(x) = \Sigma \delta w_h \Phi_h(x)$ and $\delta \log_{10}\sigma(x) = \Sigma \delta b_h \Phi_h(x)$ respectively. Gaussian priors were assigned to the parameters w_h, b_h, δw_h and δb_h; the widths of these four Gaussians were hyperparameters inferred from the data using the 'Bayesian inference using Gibbs sampling' (BUGS) software (Thomas, Spiegelhalter & Wilks 1992). This method is similar to that used by MacKay (1995). The best estimate of the difference in magnitude between the samples with cosmic time is plotted as the central solid line. The 95 per cent confidence limits are represented by the shaded region, delimited by two solid lines. The cosmological model used has $\Omega_0 = 0.3$ and $\Omega_\Lambda = 0.7$.

3 MODELLING PROCEDURES

3.1 Cosmological models

Because of the availability of the GISSEL codes of Bruzual & Charlot, the opportunity has been taken to consider a wider range of evolutionary histories of the star formation rate of radio galaxies and to couple this with an expanded range of cosmological models, in particular, those with non-zero values of the cosmological constant (Λ). Friedman world models with zero cosmological constant and $\Omega_0 = 0, 0.1, 0.3$ and 1.0 have been considered, as have a range of models with non-zero Ω_Λ. The relation between

Table 1. Parameters of the different cosmologies investigated in this paper. It is assumed that $H_0 = 50\,\mathrm{km\,s^{-1}\,Mpc^{-1}}$.

Ω_0	Ω_Λ	Age at $R = 1$ $(T_0 H_0)$	T_0 (Gyr)
1.0	0.0	0.67	13.0
0.3	0.0	0.81	15.8
0.1	0.0	0.90	17.6
0.0	0.0	1.00	19.6
0.3	0.7	0.96	18.9
0.3	0.3	0.86	16.9
0.1	0.9	1.28	25.0
0.1	0.3	0.98	19.1

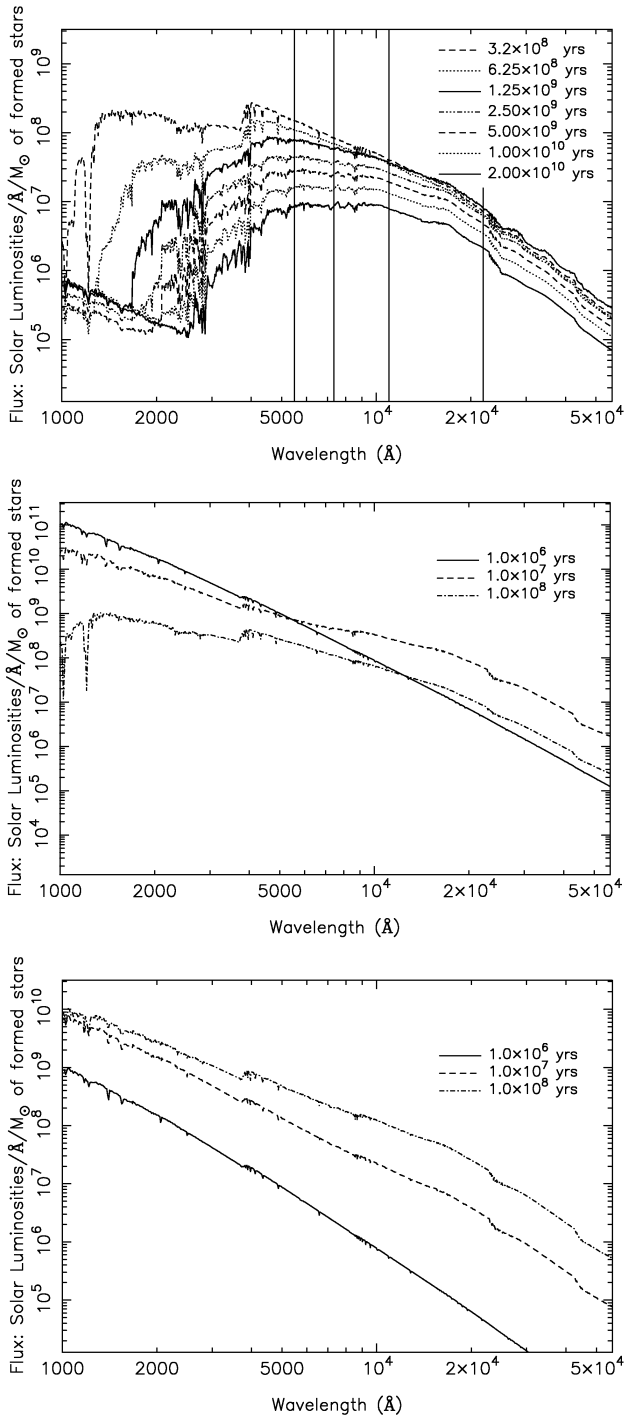

Figure 3. (a) Synthesized spectral energy distributions for the standard passive evolution model, consisting of an initial uniform starburst of duration 10^8 yr with solar metallicity, $Z = Z_\odot$. The predicted spectral energy distributions of the galaxy are displayed at eight different ages which are equally spaced logarithmically in cosmic time. The vertical lines show the regions of the spectrum corresponding to the rest wavelength of the observed K-band radiation at redshifts $z = 3, 2, 1$ and 0. (b) SEDs for the additional starbursts used in our alternative star formation histories, as described in Section 3.2. These are instantaneous starbursts, observed at ages of 10^6, 10^7 and 10^8 yr. (c) The spectral evolution of a uniform 10^8-yr starburst observed at ages 10^6, 10^7 and 10^8 yr, the spectrum at the latest time being the brightest over the full range of wavelength plotted. In all three figures, the spectra are normalized to the luminosity per unit solar mass of stars.

cosmic time and redshift is

$$t = \int_0^t \mathrm{d}t = \frac{1}{H_0}\int_z^\infty \frac{\mathrm{d}z}{(1+z)[\Omega_0(1+z)^3 + \Omega_\Lambda]^{1/2}}. \quad (1)$$

For the world models with flat geometries, $\Omega_0 + \Omega_\Lambda = 1$, corresponding to those favoured by recent analyses of the power spectrum of fluctuations in the Cosmic Microwave Background Radiation as observed in the Boomerang and Maxima experiments (e.g. Jaffe et al. 2001), there is a parametric solution:

$$t = \frac{2}{3H_0\Omega_\Lambda^{1/2}} \ln\left(\frac{1+\cos\theta}{\sin\theta}\right),$$

$$\tan\theta = \left(\frac{\Omega_0}{\Omega_\Lambda}\right)^{1/2}(1+z)^{3/2}. \quad (2)$$

Numerical integrations have been used for other models, and for determining the variation of comoving radial distance coordinate with redshift. The models with non-zero Ω_Λ considered in this analysis are listed in Table 1. Two of these have flat geometries and the other two models have open geometries with low values of both Ω_0 and Ω_Λ. This range of models with finite values of Ω_Λ spans those which would be consistent with the results found in the Supernova Cosmology project (Perlmutter et al. 1999).

3.2 Galaxy spectral synthesis

The GISSEL codes of Bruzual & Charlot provide a means of modelling galaxy spectra through isochrone synthesis. The models used in the present analysis all include the passive evolution of the stellar populations of the galaxies. The standard model is taken to have solar metallicity, $Z = Z_\odot$, and the stellar population of the galaxy was formed in an initial uniform starburst with a duration of 1.0 Gyr. The GISSEL code enabled the spectral evolution of this model to be determined for ages up to 20 Gyr, and this is shown in Fig. 3(a) at a number of ages which are equally spaced logarithmically in cosmic time. Generally, only the late stages of evolution of the starburst ($t \gg 10^9$ yr) are of interest in this analysis. For one of the models, $\Omega_0 = 0.1$ and $\Omega_\Lambda = 0.9$, the present age of the Universe, T_0, is greater than 20 Gyr, and evolution in this model was terminated at a low-redshift limit of $z = 0.3$.

It is instructive to note that, in Fig. 3(a), at optical and infrared wavelengths the spectra are roughly equally spaced logarithmically in luminosity at ages greater than 10^9 yr, indicating that, at a given wavelength, the spectral energy decreases roughly as a power-law with cosmic time. As shown by Gunn, Longair & Rees (1978), Longair (1998) and others, this power-law behaviour can be understood in terms of the rate at which stars evolve from the main sequence on to the red giant branch, if the initial mass function is assumed to be of power-law form. Such simple arguments predict that $L \propto t^{-1}$ for the $\Omega_0 = 1$, $\Omega_\Lambda = 0$ model. This is not so different from the evolution seen in Fig. 3(a), but there are important variations in the power-law index as a function of wavelength. At 0.55 μm, the evolution can be roughly described by $L_{0.5} \propto t^{-1.2}$, whereas at 2.2 μm the exponent decreases to about −0.5. Therefore, the simple approximation is not adequate for the present analysis. For essentially all our computations, only evolution at epochs greater than 10^9 yr is required. It can be seen however that at earlier times the K-band luminosity increases with age. This is associated with the evolution of stars on to the asymptotic giant branch. The stellar evolution models of Maeder & Meynet (1989) and Girardi et al. (2000) show that, for stars with $M \geq 2\,M_\odot$, as the stellar mass decreases, the luminosity of the upper asymptotic giant branch (AGB) stars increases and their temperature decreases. Thus, the simple, monotonically decreasing spectral luminosity is only applicable for times greater than 10^9 yr when the turn-off mass drops below $2\,M_\odot$ and the AGB contribution becomes less important than evolution on to the red giant branch.

In previous analyses, it was assumed that the metallicity of the galaxies corresponded to solar values. The evidence of the Madau plot in its various incarnations (see, for example, Madau, Pozzetti & Dickinson 1998) and the analyses of the metallicities of the absorption-line systems in distant quasars have suggested that the chemical abundances of the elements have evolved very significantly over the redshift interval $0 < z < 4$ (see, for example, Pettini et al. 1997). To understand the effects of metallicity upon the predicted K–z relation, models have been created for four different metallicities: $0.2\,Z_\odot$, $0.4\,Z_\odot$, $Z_\odot$, and $2.5\,Z_\odot$.

Different star formation histories have also been considered. These include a continuous exponentially decreasing star formation rate, with an e-folding time of 1 Gyr, and a simple delta-function starburst. Combined models could then be constructed involving multiple star formation events occurring at different cosmic times. For example, if the onset of radio source and quasar activity were contemporaneous with (or stimulated) an active starburst, the additional starburst component might affect the K magnitude of the galaxy. To illustrate how such events could impact the K–z relation, model starbursts can be added to the underlying passive evolution of the majority old stellar population. Two model starbursts were considered. In the first, the starburst took place instantaneously, and was observed at times 10^6, 10^7 and 10^8 yr after that event; this spectral evolution is shown in Fig. 3(b). The intriguing aspect of these spectra is that the starburst is most luminous in the infrared waveband after about 10^7 yr. After about

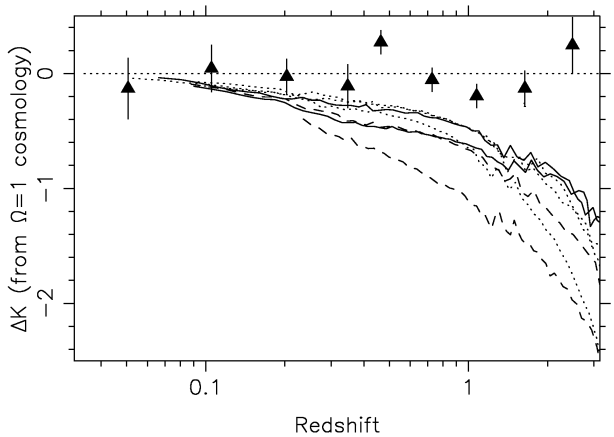

Figure 4. Changes in the predicted K–z relations for different cosmological models. The predictions are presented as differences relative to that of the $\Omega_0 = 1$, $\Omega_\Lambda = 0$ model. ΔK is defined as $K(\Omega_0 = 1) -$ K(model), so that negative values for ΔK mean that a galaxy of given absolute luminosity would be observed to have a fainter apparent magnitude. All the models include evolution of the stellar populations of the galaxies according to the standard passive evolution model. Models with $\Omega_\Lambda = 0$ and $\Omega_0 = 0.0, 0.1, 0.3$ and 1.0 are shown as dotted lines, the last model having $\Delta K = 0$ by definition; ΔK becomes more negative with decreasing Ω_0. Models with $\Omega_0 = 0.1$, $\Omega_\Lambda = 0.9$ and $\Omega_0 = 0.1$, $\Omega_\Lambda = 0.3$ are shown by dashed lines, the latter model having the more negative value of ΔK. Models with $\Omega_0 = 0.3$, $\Omega_\Lambda = 0.3$ and $\Omega_0 = 0.3$, $\Omega_\Lambda = 0.7$ are shown by solid lines, the latter model having the more negative value of ΔK. The triangles and associated error bars represent the observed values from Fig. 1.

Table 2. The cosmic time and distance coordinate D, in units of c/H_0, at which galaxies are observed in the cosmological models listed in Table 1 at redshifts 0, 1, 2 and 3. It is assumed that $H_0 = 50\,\mathrm{km\,s^{-1}\,Mpc^{-1}}$. The third line of each entry shows the contribution of the choice of cosmological model ΔK_Ω to ΔK. The fourth line shows the exact contribution of $\Delta K_{\rm ev}$ to ΔK. The fifth line shows the total value of ΔK which is derived from integration over the band pass of the K-filter.

	$\Omega_0 = 1$ $\Omega_\Lambda = 0$	$\Omega_0 = 0.3$ $\Omega_\Lambda = 0$	$\Omega_0 = 0.1$ $\Omega_\Lambda = 0$	$\Omega_0 = 0$ $\Omega_\Lambda = 0$	$\Omega_0 = 0.3$ $\Omega_\Lambda = 0.7$	$\Omega_0 = 0.3$ $\Omega_\Lambda = 0.3$	$\Omega_0 = 0.1$ $\Omega_\Lambda = 0.9$	$\Omega_0 = 0.1$ $\Omega_\Lambda = 0.3$
$z=0$	13.0 Gyr	15.8 Gyr	17.6 Gyr	19.6 Gyr	18.9 Gyr	16.9 Gyr	25.0 Gyr	19.1 Gyr
	$D=0.00$	$D=0.00$	$D=0.00$	$D=0.00$	$D=0.00$	$D=0.00$	$D=0.00$	$D=0.00$
	$\Delta K_\Omega=0.00$	$\Delta K_\Omega=0.00$	$\Delta K_\Omega=0.00$	$\Delta K_\Omega=0.00$	$\Delta K_\Omega=0.00$	$\Delta K_\Omega=0.00$	$\Delta K_\Omega=0.00$	$\Delta K_\Omega=0.00$
	$\Delta K_{\rm ev}=0.00$	$\Delta K_{\rm ev}=0.00$	$\Delta K_{\rm ev}=0.00$	$\Delta K_{\rm ev}=0.00$	$\Delta K_{\rm ev}=0.00$	$\Delta K_{\rm ev}=0.00$	$\Delta K_{\rm ev}=0.00$	$\Delta K_{\rm ev}=0.00$
	$\Delta K=0.00$	$\Delta K=0.00$	$\Delta K=0.00$	$\Delta K=0.00$	$\Delta K=0.00$	$\Delta K=0.00$	$\Delta K=0.00$	$\Delta K=0.00$
$z=1$	4.61 Gyr	6.54 Gyr	7.97 Gyr	9.80 Gyr	8.05 Gyr	7.07 Gyr	12.73 Gyr	8.89 Gyr
	$D=0.59$	$D=0.69$	$D=1.11$	$D=0.75$	$D=0.77$	$D=0.72$	$D=0.90$	$D=0.77$
	$\Delta K_\Omega=0.00$	$\Delta K_\Omega=-0.34$	$\Delta K_\Omega=-0.47$	$\Delta K_\Omega=-0.54$	$\Delta K_\Omega=-0.60$	$\Delta K_\Omega=-0.44$	$\Delta K_\Omega=-0.92$	$\Delta K_\Omega=-0.59$
	$\Delta K_{\rm ev}=0.00$	$\Delta K_{\rm ev}=-0.13$	$\Delta K_{\rm ev}=0.00$	$\Delta K_{\rm ev}=-0.11$	$\Delta K_{\rm ev}=-0.02$	$\Delta K_{\rm ev}=-0.04$	$\Delta K_{\rm ev}=-0.21$	$\Delta K_{\rm ev}=-0.07$
	$\Delta K=0.00$	$\Delta K=-0.47$	$\Delta K=-0.47$	$\Delta K=-0.65$	$\Delta K=-0.62$	$\Delta K=-0.48$	$\Delta K=-1.13$	$\Delta K=-0.66$
$z=2$	2.51 Gyr	4.34 Gyr	4.92 Gyr	6.53 Gyr	4.52 Gyr	4.07 Gyr	7.55 Gyr	5.45 Gyr
	$D=0.85$	$D=1.10$	$D=1.24$	$D=1.33$	$D=1.12$	$D=1.15$	$D=1.54$	$D=1.32$
	$\Delta K_\Omega=0.00$	$\Delta K_\Omega=-0.59$	$\Delta K_\Omega=-0.84$	$\Delta K_\Omega=-0.99$	$\Delta K_\Omega=-0.78$	$\Delta K_\Omega=-0.67$	$\Delta K_\Omega=-1.30$	$\Delta K_\Omega=-0.97$
	$\Delta K_{\rm ev}=0.00$	$\Delta K_{\rm ev}=-0.29$	$\Delta K_{\rm ev}=-0.13$	$\Delta K_{\rm ev}=-0.39$	$\Delta K_{\rm ev}=-0.10$	$\Delta K_{\rm ev}=-0.12$	$\Delta K_{\rm ev}=-0.40$	$\Delta K_{\rm ev}=-0.21$
	$\Delta K=0.00$	$\Delta K=-0.88$	$\Delta K=-0.97$	$\Delta K=-1.38$	$\Delta K=-0.88$	$\Delta K=-0.79$	$\Delta K=-1.70$	$\Delta K=-1.18$
$z=3$	1.63 Gyr	2.57 Gyr	3.46 Gyr	4.90 Gyr	2.96 Gyr	2.72 Gyr	5.04 Gyr	3.80 Gyr
	$D=1.00$	$D=1.43$	$D=1.68$	$D=1.88$	$D=1.49$	$D=1.46$	$D=1.98$	$D=1.77$
	$\Delta K_\Omega=0.00$	$\Delta K_\Omega=-0.77$	$\Delta K_\Omega=-1.13$	$\Delta K_\Omega=-1.37$	$\Delta K_\Omega=-0.86$	$\Delta K_\Omega=-0.82$	$\Delta K_\Omega=-1.48$	$\Delta K_\Omega=-1.24$
	$\Delta K_{\rm ev}=0.00$	$\Delta K_{\rm ev}=-0.72$	$\Delta K_{\rm ev}=-0.42$	$\Delta K_{\rm ev}=-0.85$	$\Delta K_{\rm ev}=-0.42$	$\Delta K_{\rm ev}=-0.37$	$\Delta K_{\rm ev}=-0.81$	$\Delta K_{\rm ev}=-0.39$
	$\Delta K=0.00$	$\Delta K=-1.49$	$\Delta K=-1.55$	$\Delta K=-2.22$	$\Delta K=-1.28$	$\Delta K=-1.19$	$\Delta K=-2.29$	$\Delta K=-1.63$

this time the most massive stars complete their evolution on the main sequence and join the asymptotic giant branch. It is interesting that the time-scale of 10^7 yr is of the same order as the typical age of the radio source events associated with the 3CR and 6C sources, so such a starburst could contribute to the K luminosity of the galaxy. In the second example the case of a constant starburst lasting 10^8 yr is considered, but observed at 10^6, 10^7 and 10^8 yr after the start of the event; these spectra are shown in Fig. 3(c). In this case, the starburst is expected to have a much smaller effect upon the K luminosity of the galaxy. It can be seen that, after 10^6 yr, the starburst has the same spectrum as the first model, but with only one hundredth of the luminosity because only that fraction of the stars have formed by that time. On the other hand, after 10^8 yr, the starburst is more luminous than in the first model because there is a significant contribution of recently formed stars to the K luminosity. In either case, it can be seen that starbursts observed between 10^7 and 10^8 yr after the onset of the starburst can have a significant impact upon the K luminosity of the galaxy. Models have been considered in which the mass fractions of newly formed stars range between 0.5 and 5.0 per cent of the total stellar mass of the galaxy.

The resulting spectral energy distributions (SEDs) were then redshifted and convolved with the transmission function of the standard K filter. These were then combined with the different world models to create K–z diagrams. A catalogue of the range of models considered is given in Tables 3 and 4, later.

4 RESULTS

4.1 Changing the cosmological model

It is simplest to illustrate the effects of changing the parameters of the cosmological models by subtracting the predicted K–z track for the chosen cosmology from the corresponding predictions of the $\Omega_0 = 1.0$, $\Omega_\Lambda = 0$ model: ΔK is defined as $K(\Omega_0 = 1) -$ K(model) so that negative values of ΔK mean that a galaxy of a given absolute luminosity would be observed to have a fainter apparent magnitude. The results for the cosmologies listed in Table 1 are shown in Fig. 4 and tabulated in Table 2.

It is instructive to distinguish those contributions to ΔK due to the choice of cosmological model and those due to the evolving spectrum of the galaxy. The latter can be thought of as the K correction including the effects of the evolution of the stellar population. Following the notation of Longair (1998), the flux density of the galaxy is given by

$$S_i(\nu_0, z) = \frac{L[\nu_0(1+z), t_i(z)]}{4\pi D_i^2(z)(1+z)} \tag{3}$$

where i labels the choice of cosmological model and $D_i(z)$ is a distance measure which is related to the standard luminosity distance $D_{\rm L}$ by $D_{\rm L} = D_i(z)(1+z)$. The luminosities of the modelled galaxies in the different cosmologies are normalized by varying their stellar mass, such that at zero redshift they have K-band luminosities $L_{\rm K(z=0)}$ matching the observed K–z relation. Therefore if $L'[\nu,t]$ is the luminosity of the galaxy per solar mass,

$$L[\nu_0(1+z), t_i(z)] = L'[\nu_0(1+z), t_i(z)] \frac{L_{\rm K(z=0)}}{L'[\nu_0, t_i(0)]}. \tag{4}$$

The ratio of the flux densities in the ith model to those in the fiducial model, for the same observed flux density at small redshifts, is given by

$$\frac{S_i(\nu_0, z)}{S_0(\nu_0, z)} = \frac{L'[\nu_0(1+z), t_i(z)]}{L'[\nu_0, t_i(0)]} \frac{L'[\nu_0, t_0(0)]}{L'[\nu_0(1+z), t_0(z)]} \frac{D_0^2(z)}{D_i^2(z)}. \tag{5}$$

Thus, the magnitude difference associated with the choice of

Table 3. Changes in the K magnitudes, ΔK, relative to the no-evolution model for four representative world models. The first part of this table gives the mean differences ΔK between the no-evolution model for these cosmologies and the observational data for all points within 20 per cent of three different redshifts. The relations have been normalized to the mean observed magnitudes at small redshifts. Positive values indicate that the data points are brighter than the no-evolution track at that redshift. The second half of the table shows the same differences once account is taken of the passive evolution of the stellar content of the galaxies. For all four cases, the standard initial starburst is taken have the following parameters: $z_f = 10$, metallicity $Z = Z_\odot$, $H_0 = 50\,\mathrm{km\,s^{-1}\,Mpc^{-1}}$, and the duration of the initial starburst 1 Gyr. Negative values indicate that the predicted evolution in K-band magnitude is less than that required by the data, that is, the modelled track is fainter than the mean of the observed relation at that redshift.

Cosmological Model	Sample	ΔK from the no-evolution track at different redshifts $z = 0.5$	$z = 1.0$	$z = 2.0$
$\Omega_0 = 1.0$, $\Omega_\Lambda = 0.0$	3CR Data	0.597 ± 0.140	1.022 ± 0.126	1.780 ± 0.114
	6C Data	0.706 ± 0.097	0.433 ± 0.145	1.136 ± 0.233
	Combined Data	0.646 ± 0.089	0.742 ± 0.115	1.222 ± 0.210
$\Omega_0 = 0.1$, $\Omega_\Lambda = 0.0$	Combined Data	0.778 ± 0.091	1.110 ± 0.118	1.945 ± 0.220
$\Omega_0 = 0.1$, $\Omega_\Lambda = 0.3$	Combined Data	0.712 ± 0.091	1.076 ± 0.119	1.925 ± 0.220
$\Omega_0 = 0.3$, $\Omega_\Lambda = 0.7$	Combined Data	0.789 ± 0.091	1.101 ± 0.117	1.758 ± 0.214
	Model	ΔK difference between model and observations		
$\Omega_0 = 1.0$, $\Omega_\Lambda = 0.0$	standard initial starburst	-0.177 ± 0.089	0.162 ± 0.115	0.336 ± 0.210
$\Omega_0 = 0.1$, $\Omega_\Lambda = 0.0$	standard initial starburst	-0.303 ± 0.091	-0.262 ± 0.118	-0.696 ± 0.220
$\Omega_0 = 0.1$, $\Omega_\Lambda = 0.3$	standard initial starburst	-0.352 ± 0.091	-0.310 ± 0.119	-0.799 ± 0.220
$\Omega_0 = 0.3$, $\Omega_\Lambda = 0.7$	standard initial starburst	-0.420 ± 0.091	-0.295 ± 0.117	-0.454 ± 0.214

cosmological model is

$$\Delta K_\Omega = 5 \log[D_i(z)/D_0(z)], \tag{6}$$

while that associated with observing different parts of the evolving spectral energy distribution at different cosmic times is

$$\Delta K_{\mathrm{ev}} = 2.5 \log \left\{ \frac{L'[\nu_0(1+z), t_i(z)]}{L'[\nu_0, t_i(0)]} \frac{L'[\nu_0, t_0(0)]}{L'[\nu_0(1+z), t_0(z)]} \right\} \tag{7}$$

The total change in magnitude is given by $\Delta K = \Delta K_\Omega + \Delta K_{\mathrm{ev}}$. Table 2 shows these differences for the models listed in Table 1.

Fig. 4 shows that galaxies are expected to be fainter at large redshifts in all the models considered, as compared with the model that has $\Omega_0 = 1$, $\Omega_\Lambda = 0$; this means that for the same observed K magnitude, the galaxies would have to be intrinsically more luminous. There are several effects which contribute to this decrease. The most important of these is the fact that, for a given redshift, galaxies are observed at greater radial comoving coordinate distances as compared with the model with $\Omega_0 = 1$, $\Omega_\Lambda = 0$. In addition, the cosmic times at which the spectral energy distributions are observed are significantly different. What is important, however, are the relative epochs at which the galaxies are observed. It turns out that, in the passively evolving models, the relative changes in observed luminosity ($\Delta \mathrm{K_{ev}}$) are significantly less than the effects of the cosmological model ($\Delta \mathrm{K}_\Omega$). This can be understood from Table 2, which shows the ages and distance coordinates at which galaxies at different redshifts are observed in the different cosmologies listed in Table 1, assuming $H_0 = 50\,\mathrm{km\,s^{-1}\,Mpc^{-1}}$; included in this table are the contributions of $\Delta \mathrm{K}_\Omega$, the total change in K magnitude ΔK and the difference between them $\Delta \mathrm{K_{ev}}$, which represents the contribution of the changing spectral energy distribution of the galaxies with cosmic epoch.

Table 2 quantitatively demonstrates the important point that, at all redshifts, the choice of cosmological model is always much more important than the evolution corrections within the context of passively evolving models for the stellar populations of the galaxies, as far as the *differences* from the fiducial model are concerned.

It is interesting that it is possible to reproduce the results of the exact computations quite accurately by interpolating the luminosity changes at the appropriate redshifted wavelength in the template spectra shown in Fig. 3(a). It is found that this approach generally produces results accurate to about 0.1 mag, which is normally accurate enough to draw useful conclusions. The value of this approach is that it enables the investigator to use Fig. 3(a) to work out quite precisely the effects of the K corrections for any other world model with any given value of Hubble's constant, and for alternative assumptions relative to the template spectral evolution shown in Fig. 3(a).

Poggianti (1997) provides tables of K corrections and evolutionary corrections for observations in a number of specific filters, assuming an $\Omega_0 = 0.45$ cosmology. We have compared these results with those of our two most similar cosmologies, i.e. $\Omega_0 = 1$, $\Omega_\Lambda = 0$ and $\Omega_0 = 0.3$, $\Omega_\Lambda = 0$. Despite a different set of spectral synthesis models, the evolutionary corrections for an elliptical galaxy formed with an e-folding time of 1 Gyr given by Poggianti are in good general agreement with our own, suggesting that the choice of stellar synthesis code does not have a large impact on the evolutionary corrections determined. The K corrections given by Poggianti for her single cosmology in the K waveband also agree well with our own results.

Considering first the range of models shown in Fig. 4, it is evident that only the passively evolving $\Omega_0 = 1$, $\Omega_\Lambda = 0$ model provides a reasonable fit to the data. The error bars shown in the figure represent the standard errors in the mean of the K magnitude of the galaxies, within the given redshift intervals, and are less than the standard deviations shown in Fig. 1 by a factor of $\sqrt{N}$, where $N \sim 10$–20.

For illustrative purposes, a quantitative comparison between four of the models plotted in Fig. 4 is given in Table 3. These are the models with $\Omega_0 = 1.0$, $\Omega_\Lambda = 0.0$; $\Omega_0 = 0.1$, $\Omega_\Lambda = 0.0$; $\Omega_0 = 0.1$, $\Omega_\Lambda = 0.3$; and $\Omega_0 = 0.3$, $\Omega_\Lambda = 0.7$. In the first part of the table, the magnitude difference, ΔK, between the data points and the no-evolution tracks at redshifts $z = 0.5, 1.0$ and 2.0 are

Table 4. Changes in the K magnitudes, ΔK, relative to the standard passive evolution model in an $\Omega_0 = 1$, $\Omega_\Lambda = 0$ world model for the representative world models. Results are given for redshifts $z = 0.5$, 1.0 and 2.0. Positive values of ΔK, which is defined as $K_0 - K_{\rm model}$, indicate that the new model results in a greater increase in infrared luminosity as compared with the standard passive evolution model.

Section		ΔK from the observational data: $z = 0.5$	$z = 1.0$	$z = 2.0$
	Standard Passive Evolution Model: $\Omega_0 = 1.0$, $\Omega_\Lambda = 0.0$, $z_{\rm f} = 10$, $Z = Z_\odot$ 1-Gyr starburst, $H_0 = 50\,{\rm km\,s^{-1}\,Mpc^{-1}}$.	−0.18	0.16	0.34
	Change from standard passive evolution model	ΔK difference from standard passive evolution model: $z=0.5$	$z=1.0$	$z=2.0$
(4.1)	$\Omega_0=0.1$, $\Omega_\Lambda=0.0$	−0.13	−0.42	−1.03
	$\Omega_0=0.1$, $\Omega_\Lambda=0.3$	−0.18	−0.47	−1.14
	$\Omega_0=0.3$, $\Omega_\Lambda=0.7$	−0.24	−0.46	−0.79
(4.2)	$z_{\rm f}=2$	0.10	0.27	–
	$z_{\rm f}=3$	−0.00	0.10	0.57
	$z_{\rm f}=5$	−0.02	0.04	0.14
	$z_{\rm f}=10$	0.00	0.00	0.00
	$z_{\rm f}=20$	−0.04	−0.05	−0.14
	$z_{\rm f}=100$	0.00	−0.02	−0.12
(4.3)	$H_0=50\,{\rm km\,s^{-1}\,Mpc^{-1}}$	0.00	0.00	0.00
	$H_0=65\,{\rm km\,s^{-1}\,Mpc^{-1}}$	−0.02	0.04	−0.01
	$H_0=100\,{\rm km\,s^{-1}\,Mpc^{-1}}$	−0.01	−0.05	0.12
(4.4)	$Z=0.2\,Z_\odot$	0.05	0.22	0.45
	$Z=0.4\,Z_\odot$	0.09	0.10	0.32
	$Z=1.0\,Z_\odot$	0.00	0.00	0.00
	$Z=2.5\,Z_\odot$	0.13	−0.04	−0.16
(4.5)	Instantaneous SFR	−0.04	−0.09	−0.21
	1-Gyr constant rate	0.00	0.00	0.00
	Exponential SFR	0.05	0.07	0.05
(4.5)	Extra starburst, 2.5 per cent mass, 10^6 yr old	0.04	0.07	0.17
	Extra starburst, 2.5 per cent mass, 10^7 yr old	0.32	0.28	0.22
	Extra starburst, 2.5 per cent mass, 10^8 yr old	0.04	0.04	0.05
(4.5)	Extra starburst, 10^7 yr old, 0.5 per cent mass	0.07	0.06	0.05
	Extra starburst, 10^7 yr old, 1.0 per cent mass	0.14	0.12	0.09
	Extra starburst, 10^7 yr old, 2.5 per cent mass	0.32	0.28	0.22
	Extra starburst, 10^7 yr old, 5.0 per cent mass	0.56	0.50	0.40

listed, and in the second the difference in ΔK between the data points and the passive evolution models of Fig. 4 are shown. These data are also included as the first two entries in Table 4. The K–z relations have been normalized to the same K magnitude at low redshift for both the passive evolution and the no-evolution tracks, because the mean magnitudes of the galaxies at $z < 0.3$ are consistent with a very well-defined linear K–z relation, as can be seen from Fig. 1. Positive values of ΔK indicate that the predicted magnitudes correspond to brighter galaxies than are needed to account for the data. For example, the $\Omega_0 = 1.0$, $\Omega_\Lambda = 0$ model results in slightly brighter tracks than the mean of the data points at $z = 2.0$.

The importance of these results is that, in general, except for the fiducial model ($\Omega_0 = 1$, $\Omega_\Lambda = 0$) the galaxies are predicted to be fainter at large redshifts than they are observed to be, even when passive evolution is taken into account. This is a somewhat unexpected result. First of all, according to the hierarchical clustering model, galaxies at large redshifts should be less luminous than those nearby as they contain fewer stars. The present results go in entirely the wrong direction. For the most extreme T_0H_0 models, the galaxies would need to contain about 10 times more stars to account for these differences. Secondly, it might be argued that this result would be found if there were a correlation between radio luminosity and the K luminosity of the galaxy. In this case, the galaxies at large redshift would be expected to be larger than those at small redshifts. The analysis of McLure & Dunlop (2000) showed, however, that the half-width diameters of the luminosity profiles of the radio galaxies are invariant as a function of redshift, suggesting that the galaxies have attained a similar evolutionary state as far as their total stellar populations are concerned.

Because of these somewhat surprising conclusions, the impact of changing the assumptions made in the fiducial model in plausible ways has been analysed in more detail.

4.2 Star formation epoch

The epoch at which the stellar populations were formed was

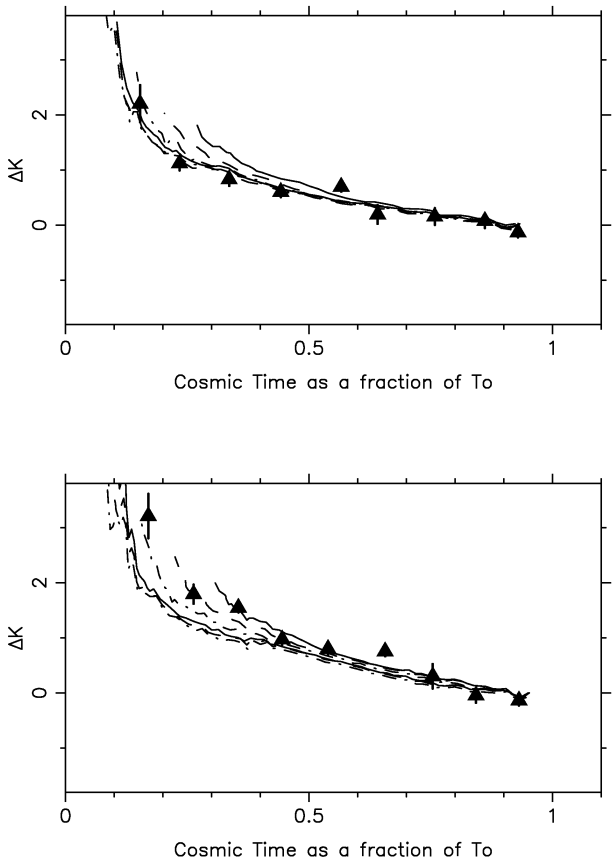

Figure 5. The values of ΔK relative to the no-evolution model as a function of cosmic time, for galaxies with different assumed values of the redshifts, z_f, at which their stellar populations formed for (a) the critical model, $\Omega_0 = 1$, $\Omega_\Lambda = 0$ and (b) a flat model with $\Omega_0 = 0.3$, $\Omega_\Lambda = 0.7$. In both plots, the upper solid line corresponds to $z_f = 2$, the upper dashed line to $z_f = 3$, the upper dot-dashed line to $z_f = 5$, the lower solid line to $z_f = 10$, the lower dashed line to $z_f = 20$ and the lower dot-dashed line to $z_f = 100$. In both plots it is assumed that the stars are formed in a 1-Gyr starburst during which the star formation rate is constant. Solar metallicity is assumed. The mean values of the observed values of ΔK in equal cosmic time intervals of $0.1T_0$ are plotted as in Fig. 1, with error bars corresponding to the standard error in the mean of the K magnitudes of both sets of observational data.

allowed to vary between redshifts of 2 and 100. The sense of the changes to the K–z relations are similar for all cosmological models. Fig. 5 shows the K-band magnitude differences of the models relative to the no-evolution track in the same cosmology for models with $\Omega_0 = 1$, $\Omega_\Lambda = 0$ and $\Omega_0 = 0.3$, $\Omega_\Lambda = 0.7$. The magnitude differences relative to the fiducial model are listed in Table 4 for $\Omega_0 = 1$, $\Omega_\Lambda = 0$. Results have not been tabulated for models with $\Omega_0 = 0.3$, $\Omega_\Lambda = 0.7$, as the magnitude differences within these models were not dissimilar to those in the Einstein–de Sitter cosmology. In Fig. 5, the values of ΔK are plotted against cosmic time as a fraction of T_0, where T_0 is the present age of the Universe listed in Table 1 for $H_0 = 50\,\mathrm{km\,s^{-1}\,Mpc^{-1}}$.

In Fig. 5, it is assumed that the galaxies have solar metallicity. All models have been normalized to the same magnitude at the lowest redshifts, at which the mean K–z relation is well defined. The models diverge at earlier times. As expected, if the epoch of star formation is less than the reference value $z_f = 10$ the predicted tracks are more luminous at redshifts $z \sim 2$–3. The largest differences occur in the cases in which the star formation is assumed to begin at $z_f = 2$ and 3, these being less than that at which radio galaxies are known to exist. None the less, it is noteworthy that, unless the epoch of star formation were as unreasonably low as $z_f = 2$–3, changing the epoch of star formation does not result in a particularly large change in ΔK. The reason for this can be understood from Fig. 3(a). By adopting 2.2 μm as the wavelength at which the magnitude–redshift relation is determined, even at redshift $z = 3$ the changes in the luminosity of the galaxies at a rest wavelength of 500 nm are quite small and change monotonically with time. Indeed, the difference between observing the starburst at ages 0.32 to 1.25×10^9 yr amounts to less than a factor of 3 at 5000 Å in the rest frame. This behaviour contrasts dramatically with what would be expected if the redshift–magnitude relation were determined in, say, the R waveband. Then, Fig. 3(a) shows that the variations in luminosity at rest-frame wavelengths of 1500 Å would be very sensitive to even small amounts of ongoing star formation. These calculations illustrate the considerable advantages of carrying out studies of the redshift magnitude relation in the K waveband – the observations provide information about the bulk star formation activity of the galaxies more directly.

As expected, as z_f increases the predicted K–z relations become fainter at large redshifts and there is little difference between the tracks in both models if z_f is greater than 10. In the case of the model $\Omega_0 = 0.3$, $\Omega_\Lambda = 0.7$, the fit to the data can be improved considerably if the star formation redshift $z_f \sim 3$–5 is adopted. Values of ΔK for the examples given in Fig. 5(a) at redshifts of 0.5, 1.0 and 2.0 are included in Table 4.

4.3 The value of Hubble's constant

Intuitively, it would seem that the choice of Hubble's constant would have a significant impact upon the form of the K–z relation, because the cosmic time-scale is significantly different if, say, H_0 were as large as $100\,\mathrm{km\,s^{-1}\,Mpc^{-1}}$. Then, all cosmic time-scales would be reduced by a factor of 2, allowing much less time for the evolution of the stellar populations of the galaxies and also observing them at very much earlier times at large redshifts. These changes, as well as those for $H_0 = 65\,\mathrm{km\,s^{-1}\,Mpc^{-1}}$, are given in Table 4. In the cases of models with larger values for H_0, an initial starburst of very short duration was adopted so that the galaxy is observed during the passive evolution phase; the tabulated values in Table 4 have included this change in star formation history.

It is noteworthy that changing the value of Hubble's constant has a remarkably small effect upon the predicted evolutionary tracks. The reasons for this can be understood from an inspection of Fig. 3(a). As was emphasized in Section 3.2, as long as the analysis is restricted to redshifts of less than 3, the spectral evolution of the stellar energy distribution is monotonic with time and can be reasonably described by power laws at different wavelengths from 0.5 to 2.2 μm. Thus, if the value of Hubble's constant is changed, the stellar mass of the galaxies required to normalize the K–z relation at low redshift is changed, but the differences in the values of ΔK_{ev} depend primarily upon the changing *relative* cosmic times observed at different redshifts. In general, these are quite small, so changing the value of H_0 does not greatly change the evolutionary corrections. If the redshift magnitude relation were determined at rest-frame ultraviolet (UV) wavelengths, this would certainly not be the case.

4.4 Varying the metallicity of the galaxies

The metallicity of the galaxies can significantly influence their

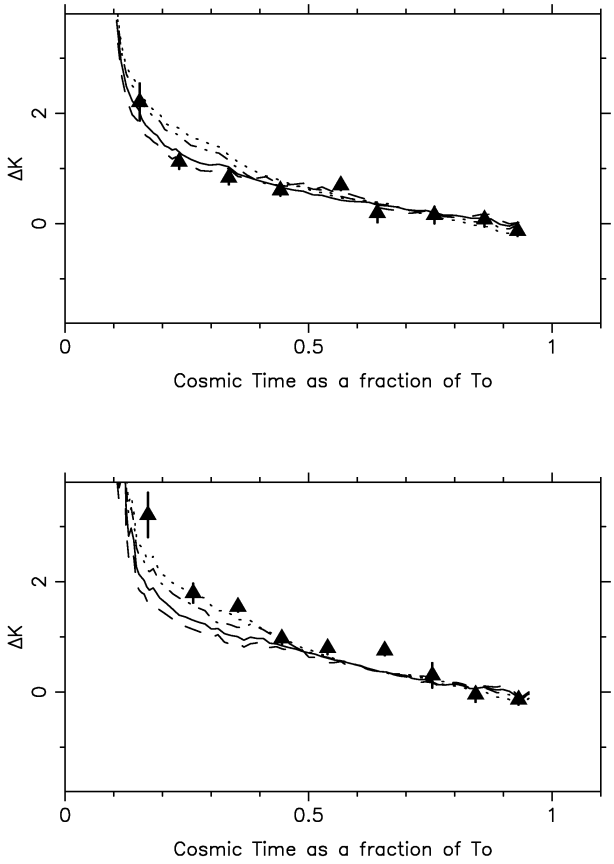

Figure 6. The values of ΔK as a function of cosmic time relative to the no-evolution model for different assumed metallicities for (a) the critical model, $\Omega_0 = 1$, $\Omega_\Lambda = 0$ and (b) a flat model with $\Omega_0 = 0.3$, $\Omega_\Lambda = 0.7$. The ΔK cosmic time relations for the different metallicities are as follows: dotted line $Z = 0.2\,Z_\odot$; dot-dashed line $Z = 0.4\,Z_\odot$; solid line $Z = Z_\odot$ and dashed line $Z = 2.5\,Z_\odot$. The models involve a 1-Gyr constant starburst, in which star formation begins at $z_f = 10$. Symbols are as in Fig. 5.

evolutionary tracks. Rather than attempting to adopt some arbitrary chemical history, the evolutionary codes have been run for metallicities of $0.2\,Z_\odot$, $0.4\,Z_\odot$, $Z_\odot$ and $2.5\,Z_\odot$. The results are displayed in Fig. 6 for the same two cosmologies discussed in Section 4.2 and for $z_f = 10$. For the Einstein–de Sitter cosmology, these results are also tabulated in Table 4. All four K–z tracks are normalized to the same magnitude scale as the fiducial model, rather than to the same magnitude at the present epoch. This procedure has been adopted so that at all times the variations due to changes in metallicity are clearly displayed. The sense of the changes is that the lower the metallicity, the more luminous the galaxy at early epochs. It is apparent from Fig. 6(b) that assuming a lower metallicity at large redshifts improves the fit of the $\Omega_0 = 0.3$, $\Omega_\Lambda = 0.7$ model as compared with the fiducial model.

The lowest metallicity track is initially the brightest (largest ΔK), and the $2.5\,Z_\odot$ track is the faintest, but the tracks cross over at low redshift. The greatest variation between the tracks occurs at early epochs and, as we have seen from Section 3.2, it is at these young ages that the galaxies undergo the greatest amount of evolution. The early evolution of the spectral energy distribution is highly sensitive to the metallicity of the galaxy because, for a star of a given mass, changing the metallicity leads to a change in the age at which it moves from the main sequence on to the AGB; for lower values of $Z/Z_\odot$ the stars evolve more rapidly because there is

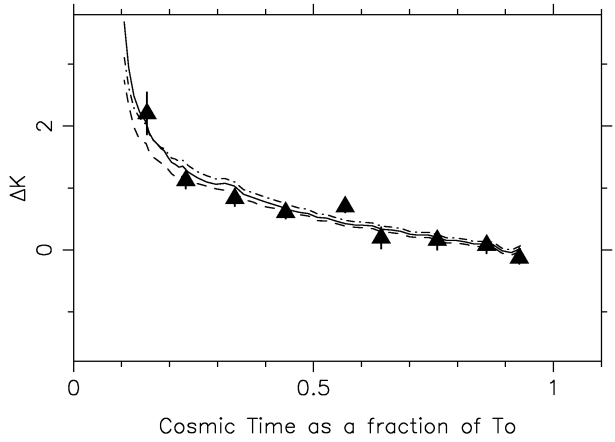

Figure 7. The values of ΔK as a function of cosmic time relative to the no-evolution model for the critical model ($\Omega_0 = 1$, $\Omega_\Lambda = 0$), for galaxies modelled with different star formation histories. Dashed line: instantaneous starburst. Solid line: 1-Gyr starburst with constant star formation rate. Dot-dashed line: exponentially decaying starburst with 10^9 year e-folding time-scale. Galaxies are modelled assuming solar metallicity, and $z_f = 10$. Symbols are as in Fig. 5(a).

less line blanketing and lower opacity. This has two consequences: first, the more rapid evolution means that lower metallicity stars were more luminous at early times; secondly, the stars were also shorter-lived and at later times there are fewer stars present in the older galaxies, which therefore appear fainter than a higher metallicity galaxy of a similar age.

It is interesting that the divergence of the different metallicity tracks occurs when the Universe was roughly half its present age, corresponding to the redshift at which the K–z relations for the 3CR and 6C samples begin to diverge. It is just conceivable that such an effect could account for the difference between these samples, but it would require those 6C galaxies which are less luminous than the 3CR galaxies to have higher metallicities. There is no obvious reason why greater radio luminosity should be correlated with lower metallicity of the stellar populations of the radio galaxies.

The diagrams in Fig. 6 can be used to construct approximate evolving galaxy models in which the metallicities of the galaxies increase with cosmic epoch. Such evolution tracks can be found by changing from one locus to another as the metallicity increases. The range of models shown in Fig. 6 illustrates how such changes would alter the predicted K–z relations.

4.5 Star formation history

The results so far have involved an initial starburst during which the star formation rate has been assumed to be constant. It is also important to consider models in which there is ongoing star formation, and in particular those in which the occurrence of a radio source event might be associated with a major star formation event in the host galaxy. This could occur if, for example, the central black hole were fuelled following some form of galaxy merger. To understand the significance of these results, we need to look more closely at the origin of the K-band flux density.

The K-band luminosity of evolving galaxies arises from two stellar populations. Stars with mass $M \gtrsim 2\,M_\odot$ evolve beyond core and shell helium burning to become asymptotic giant stars; those with $M \lesssim 2\,M_\odot$ become red giant stars and form the old red giant branch seen, for example, in globular clusters. In the present study,

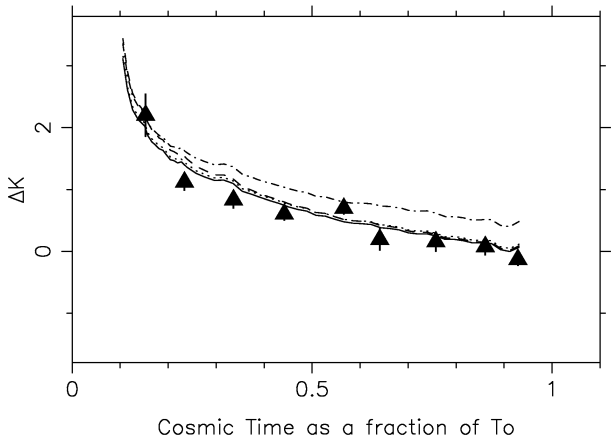

Figure 8. Changing ΔK with age of the universe, for galaxies modelled with complex star formation histories with an additional starburst occurring a fixed time before the observations, as outlined in Section 2.2. The plotted tracks represent the following models: solid line – no additional starburst; dashed line – additional starburst occurring 10^6 yr prior to the observations; dot-dashed line – starburst 10^7 yr old; and dotted line – starburst 10^8 yr old. Galaxies are modelled with solar metallicity, and $z_f = 10$, in an Einstein–de Sitter universe. The extra starburst accounts for 2.5 per cent of the total stellar mass of the galaxy. Symbols are as in Fig. 5.

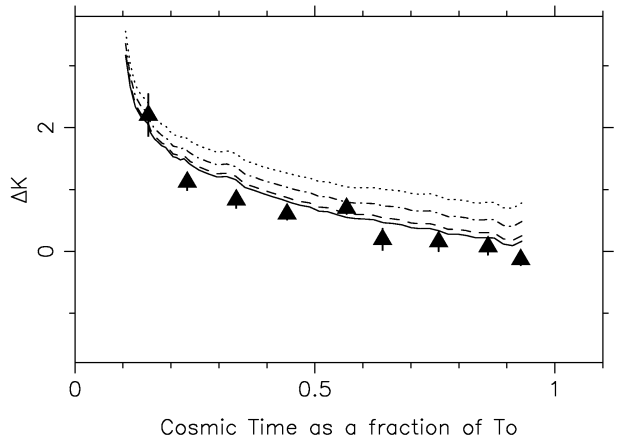

Figure 9. Changing ΔK with age of the universe, for galaxies modelled with star formation histories similar to those in Fig. 8. The plotted tracks represent models with the following stellar mass fractions involved in the extra starburst: solid line – 0.5 per cent; dashed line – 1.0 per cent; dot-dashed line – 2.5 per cent; dotted line – 5.0 per cent. Galaxies are modelled with solar metallicity, and $z_f = 10$, in an Einstein–de Sitter universe. The extra starburst is modelled as occurring 10^7 yr before the observations were made. Symbols are as in Fig. 5.

we are mainly interested in the evolution of the overall stellar population of the galaxies over cosmic time-scales greater than 10^9 yr. This age corresponds to the main-sequence lifetime of a star of mass $2\,M_\odot$. Therefore, at ages greater than 10^9 yr, the evolution is dominated by stars evolving on to the standard red giant branch and the arguments given in Section 3.2 can account for the decreasing luminosity of the galaxy. On the other hand, if there are epochs of rapid star formation, the bulk of the near-infrared luminosity is associated with stars on the asymptotic giant branch. For the most luminous stars, evolution on to the asymptotic giant branch takes place after a few 10^6 yr. Fig. 3(b) dramatically shows the large increase in K luminosity of an instantaneous starburst when it is about 10^7 yr old, associated with the formation of AGB stars. On the other hand, if the starburst is of longer duration, say 10^8 yr as illustrated in Fig. 3(c), the effect is somewhat diluted by the continued formation of all types of massive stars.

Considering first variations in the long-term star formation history of the galaxy populations, Fig. 7 displays three different types of star formation history: (i) the standard 1-Gyr starburst, (ii) an instantaneous starburst of negligibly short duration, and (iii) a model in which the star formation rate decays exponentially with an e-folding time of 10^9 yr. There is very little difference between the three models, all three of which have been normalized to the same stellar mass at late cosmic times.

The brightest model (largest ΔK), except at the very earliest times, is the exponential star formation model, and the faintest is the instantaneous burst model. These results are not surprising because it is only the behaviour after 10^9 yr which is relevant to the K–z relation for $z \leq 3$. Once star formation ceases, the continued star formation of the exponential model, and sustained production of AGB stars (albeit in small numbers), is sufficient to make this model the brightest track at low redshift. The most evolved model, the instantaneous starburst, has the lowest luminosity at low redshift. These differences between the models are very small, as can be seen from the values given in Table 4.

Fig. 8 shows the standard model coupled with the SEDs of instantaneous starbursts at three different ages (10^6, 10^7 and 10^8 yr old), the additional starburst accounting for 2.5 per cent of the total stellar mass of the galaxy. The model with the additional burst occurring the longest time before observations, 10^8 yr, gives the least change from the predictions of the underlying model. Similarly, the 10^6-year-old recent burst also results in only a slight difference at low redshift. In the first case, the additional young (10^8 yr old) high-mass stars have evolved beyond the AGB, and in the second case (10^6 yr old) they have not yet had enough time for their evolution to reach that stage. Fig. 3 shows that the rest-frame K-band flux of an evolved instantaneous burst at these ages is much closer to that for the underlying star formation model than the 10^7-year-old track. At high redshift, however, we need to consider a somewhat bluer rest-frame wavelength region. Whilst there is a small difference for the 10^8-year-old model, the 10^6-year-old recent burst is slightly brighter still, which is seen in Fig. 8. The model with the 10^7-year-old recent burst component shows the greatest change from the standard model, as expected from Fig. 3. The ΔK values for these models given in Table 4 are solely due to the additional recent burst component. The additional burst consistently brightens the K–z tracks at late times. The reason for the effect being most pronounced at small redshifts is that the luminosity of the starburst is assumed to be independent of redshift. As the K luminosity increases in a roughly power-law fashion with increasing redshift, the luminosity of the starburst is soon swamped by the majority population of red giant branch stars. Fig. 9 displays the results for the same set of models as in Fig. 8, but the mass fraction of the additional starburst is varied rather than its age. The tracks in this figure involve an additional 10^7-yr starburst and four mass fractions.

If the mass of the starburst as a function of redshift remains constant, the overall shape of the K–z relation is flattened at late times and does not result in an improved fit to the observational data. Some scatter might be introduced into the K–z relation, because the radio galaxies are observed at a range of ages from 10^6 to 10^8 yr. In order for starbursts to change the shapes of the K–z relations significantly, the additional starburst mass would need to change with redshift. This is quite possible, as there is more gas available in any merger-induced starburst at high redshift. The

same would be true if the starburst were radio-jet induced (e.g. Rees 1989), which provides a possible explanation of the alignment effect (McCarthy et al. 1987, 1995; Chambers, Miley & van Breugel 1987). Figs 8 and 9 can be used to estimate how significantly the *K*-band luminosity could have changed if the magnitude of the starburst were to vary with cosmic epoch. Just as in the case of evolving metallicity, so in the case of evolving starbursts; the evolutionary history can be estimated by moving from one track to another in Figs 8 and 9. For example, in Fig. 9, if the early starbursts involved 5 per cent of the galaxy mass, the evolutionary track would begin on the dotted line; if this subsequently decreased to 2.5 per cent and 1 per cent, the track would change to the dot-dashed and dashed lines respectively. A 5 per cent starburst by mass is the absolute maximum allowable given the constraints of the observed ultraviolet luminosities for the 3CR radio galaxies at $z \sim 1$ (e.g. Best et al. 1998b). In this extreme case the magnitude increase in K is at most about 0.5 mag.

5 DISCUSSION AND CONCLUSIONS

The above analyses of the *K*–*z* relations for a wide range of plausible cosmological models have established a number of useful general rules concerning the potential use of the luminosities of massive galaxies as standard candles. The value of carrying out these studies in the *K* waveband at 2.2 μm for redshifts $z \leq 3$ is clearly illustrated by the synthesized spectral energy distributions shown in Fig. 3(a), in which it can be seen that the evolution of the dominant stellar populations can be predicted with some confidence. As has been discussed by previous authors, the dominant evolutionary trends are associated with the evolution of stars in the mass range 1–2 $M_\odot$ from the main sequence on to the red giant branch. An equally important result is that, over this range of redshifts, the choice of cosmological model is much more important than the corrections associated with the evolution of the stellar populations of the galaxies, as is vividly illustrated by the values in Table 2. Thus, provided standard galaxies can be identified over the redshift range $0 \leq z \leq 3$, there are good prospects for obtaining useful information about the choice of cosmological model.

The problem with this programme is the identification of such a class of standard galaxy, particularly in the light of the favoured picture of hierarchical clustering to account for the formation of structures such as galaxies and clusters of galaxies over the same redshift interval. The analysis of Best et al. (1998a) showed that the 3CR radio galaxies seemed to form a population of galaxies of constant mass within the framework of the $\Omega_0 = 1, \Omega_\Lambda = 0$ world model, although they described a number of reasons why this was a somewhat surprising result. The present calculations have extended that analysis to a much wider range of cosmological models and considered in more detail the effects of the evolution of the stellar populations of the galaxies. The results shown in Fig. 4 and documented in Table 2 show that all the new models are a significantly poorer fit to the large redshift data. In particular, the principal cause of the poorer fits is the choice of cosmological model. Expressed in physical terms, in the critical $\Omega_0 = 1, \Omega_\Lambda = 0$ model, galaxies at a given redshift are observed at significantly smaller distance measures than in all the other models considered and so have the brightest *K* magnitudes. In all the other models considered, a literal interpretation of the results would be that the radio galaxies at redshifts $z > 1$ have greater stellar masses than the radio galaxies nearby. The analysis has shown that this result is independent of the choice of Hubble's constant.

It is of particular interest to find ways in which the favoured flat cosmological model with $\Omega_0 = 0.3$, $\Omega_\Lambda = 0.7$ can be reconciled with the observational data. As the results in Table 4 indicate, to produce an improved fit to the observational data one or more of the following changes to the standard evolution picture must be introduced:

(i) A lower redshift of star formation, $3 < z_f < 4$, provides a much improved fit to the observed *K*–*z* relation for this cosmological model (Fig. 5b). A problem with this improved fit is that the galaxies would then be expected to be very much more luminous in optical wavebands with significant evidence for younger stellar populations, whilst the red colours of distant radio galaxies suggest a much larger luminosity-weighted stellar age (cf. Dunlop et al. 1996, for example). Further, the observation of well-formed galaxies which are powerful radio sources out to redshift $z = 5.19$ (van Breugel et al. 1999) indicates that at least some of these galaxies formed at higher redshifts.

(ii) The metallicities of the galaxies may have been significantly less at redshifts $z \sim 2$ than they are at the present epoch. As shown in Fig. 6(b), decreasing the metallicity of the galaxy to only about 20 per cent of the present cosmic value significantly improves the fit of the model to the observations.

(iii) Starbursts associated with the radio source events can lead to a significant enhancement of the *K*-band luminosities of the galaxies, as a result of the rapid evolution of luminous massive stars on to the asymptotic giant branch. This could potentially improve the fit of the models in lambda cosmologies if associated starbursts brighten the distant galaxies, but not those at redshifts less than 1. This is quite plausible as such starbursts could be enhanced at high redshifts as a result of the extra gas available at these epochs for forming stars, either in a galaxy merger or triggered by the radio jet; indeed additional blue luminosity is observed in powerful radio galaxies at high redshifts (the alignment effect). There is clearly much scope for arbitrarily adjusting the masses, time-scales and cosmic evolution of the starbursts to improve the fit to the *K*-band data. However, the excess blue luminosity associated with the alignment effect requires only a few 10^9 $M_\odot$ of newly formed stars (<5 per cent of the galaxy mass), even if it were all to be associated with star formation activity (e.g. Dunlop et al. 1989; Best et al. 1998b): this sets a strong constraint upon the luminosities and durations of the bursts.

The alternative approach is to accept that, even after accounting for stellar evolution, the radio galaxies at $z \geq 1$ may indeed be more luminous, that is, have a greater stellar mass, than those at small redshifts. This conclusion would mean that the low and high redshift radio galaxies would not form a single evolving population, and would be surprising in terms of hierarchical clustering scenarios according to which such massive galaxies at high redshift are extremely rare. Given the growing evidence that the distant radio galaxies belong to cluster environments, it may be plausible that they had undergone more mergers than the nearby radio galaxies, which are found in more rarified environments: this possibility could be tested by carrying out cross-correlation analyses of radio galaxies of different *K* luminosities with field galaxies, although this becomes a demanding project for the radio galaxies at $z \geq 1$. The similar characteristic sizes of the 3CR radio galaxies at redshifts 1 and 0, however, sets constraints upon the intrinsic differences in luminosities which effectively rule out the most extreme cosmological models, those with $T_0 H_0 \gtrsim 1$.

ACKNOWLEDGMENTS

This work was supported in part by the Formation and Evolution of Galaxies network set up by the European Commission under contract ERB FMRX–CT96–086 of its TMR programme. KJI acknowledges the support of a PPARC research studentship. PNB would like to thank the Royal Society for generous financial support through its University Research Fellowship scheme.

REFERENCES

Arimoto N., Kodama T., 1996, in da Costa L. N., Renzini A., eds, Proc. ESO Workshop (November 1996), Galaxy Scaling Relations. Springer-Verlag, Berlin, p. 132
Best P. N., Longair M. S., Röttgering H. J. A., 1997, MNRAS, 292, 758
Best P. N., Longair M. S., Röttgering H. J. A., 1998a, MNRAS, 295, 549
Best P. N. et al., 1998b, MNRAS, 301, L15
Bower R. G., Kodama T., Terlevich A., 1998, MNRAS, 299, 1193
Bruzual G., Charlot S., 1993, ApJ, 405, 538
Chambers K. C., Miley G. K., van Breugel W. J. M., 1987, Nat, 329, 604
Dunlop J. S., Peacock J. A., Savage A., Lilly S. J., Heasley J. N., Simon A. J. B., 1989, MNRAS, 238, 1171
Dunlop J., Peacock J., Spinrad H., Dey A., Jimenez R., Stern D., Windhorst R., 1996, Nat, 381, 581
Eales S. A., 1985, MNRAS, 217, 149
Eales S. A., Rawlings S., 1996, ApJ, 460, 68
Eales S. A., Rawlings S., Law-Green D., Cotter G., Lacy M., 1997, MNRAS, 291, 593
Gunn J. E., Longair M. S., Rees M. J., 1978, 8th Advanced Course of the Swiss Society of Astronomy and Astrophysics (SSAA), Observational Cosmology. Geneva Observatory Publications, Geneva
Girardi L., Bressan A., Bertelli G., Chiosi C., 2000, A&AS, 141, 371
Jaffe A. H. et al., 2001, Phys. Rev. Lett., 86, 3475
Laing R. A., Riley J. M., Longair M. S., 1983, MNRAS, 204, 151
Lilly S. J., Longair M. S., 1984, MNRAS, 211, 833
Lilly S. J., McLean I. S., Longair M. S., 1984, MNRAS, 209, 401
Longair M. S., 1998, Galaxy Formation. Springer-Verlag, Berlin
MacKay D. J. C., 1995, ICANN '95 Proc. EC2 and Cie, Paris, p. 331
Madau P., Pozzetti L., Dickinson M., 1998, ApJ, 498, 106
Maeder A., Meynet G., 1989, A&A, 210, 155
McCarthy P. J., 1999, in Röttgering H., Best P. N., Lehnert M. D., eds, Proc. Coll. Amsterdam, The most distant radio galaxies. R. Netherlands Acad. Arts and Sciences, p. 5
McCarthy P. J., van Breugel W. J. M., Spinrad H., Djorgovski S., 1987, ApJ, 321, L29
McCarthy P. J., Spinrad H., van Breugel W. J. M., 1995, ApJS, 99, 27
McCarthy P. J., Kapahi V. K., van Breugel W., Persson S. E., Athreya R. M., Subrahmanya C. R., 1996, ApJS, 107, 19
McLure R. J., Dunlop J. S., 2000, MNRAS, 317, 249
Pei Y. C., Fall S. M., Hauser M. G., 1999, ApJ, 522, 604
Perlmutter S. et al., 1999, ApJ, 517, 565
Pettini M., Smith L. J., King D. L., Hunstead R. W., 1997, ApJ, 486, 665
Poggianti B. M., 1997, A&AS, 122, 399
Rees M. J., 1989, MNRAS, 239, 1P
Sandage A., 1972, ApJ, 173, 485
Stanford S. A., Eisenhardt P. R., Dickinson M., 1998, ApJ, 492, 461
Thomas A., Spiegelhalter D. J., Gilks W. R., 1992, in Bernardo J. M., Berger J. O., Dawid A. P., Smith A. F. M., eds, Bayesian Statistics 4. Clarendon Press, Oxford, p. 837
van Breugel W. J. M., Stanford S. A., Spinrad H., Stern D., Graham J. R., 1998, ApJ, 502, 614
van Breugel W. J. M., De Breuck C., Stanford S. A., Stern D., Röttgering H. J. A., Miley G., 1999, ApJ, 518, L61

This paper has been typeset from a TEX/LATEX file prepared by the author.